

# Sliding mode control for speed loop combined with MTPA strategy of IPMSM applied in electric vehicles

An Thi Hoai Thu Anh<sup>1</sup>, Tran Hung Cuong<sup>2</sup>, Duong Minh Chien<sup>1</sup>

<sup>1</sup>Department of Electrical Engineering, Faculty of Electrical and Electronics Engineering, University of Transport and Communications, Hanoi, Vietnam

<sup>2</sup>Department of Electrical Engineering, Faculty of Electrical and Electronic Engineering, Thuyloi University, Hanoi, Vietnam

## Article Info

### Article history:

Received Apr 4, 2024

Revised Oct 8, 2024

Accepted Nov 19, 2024

### Keywords:

Electric vehicles

Flux weakening region

Interior permanent magnet synchronous motor

Maximum torque per ampere strategy

Sliding mode control

## ABSTRACT

The interior permanent magnet synchronous motor (IPMSM) 's outstanding features, such as quick torque mobility capability, broad speed adjustability, robust mechanical structure, and high efficiency, make it particularly suitable for electric vehicle propulsion systems. This paper proposes a speed loop utilising the sliding mode control (SMC) with exponential reaching law and proportional-derivative term-ks, facilitating quicker transient responses and enhancing system stability. Moreover, coupling with the maximum torque per ampere strategy (MTPA) on current to improve motor torque in flux weakening region and to extend the adjustable range of motor speed for electric vehicle propulsion systems is discussed. Furthermore, with the proposed control methods and strategies, the system achieves stability despite environmental noise and uncertainties caused by uncertain parameters. Finally, simulation results conducted on MATLAB/Simulink software verify the correctness of the proposed control methods.

This is an open access article under the [CC BY-SA](https://creativecommons.org/licenses/by-sa/4.0/) license.



## Corresponding Author:

Tran Hung Cuong

Department of Electrical Engineering, Faculty of Electrical and Electronic Engineering, Thuyloi University  
Hanoi, Vietnam

Email: cuongth@tlu.edu.vn

## 1. INTRODUCTION

Electric vehicles are emerging as a means of transportation with many prominent advantages over conventional gasoline or diesel vehicles due to reduced air pollution and sound performance [1], [2]. Among traction motors: direct current (DC) motor, induction motor (IM), reluctant motor, and interior permanent magnet synchronous motor (IPMSM) are used for electric vehicles [3]-[6], the IPMSM is the most suitable because of its productivity, large speed range, and dimension [7]. The widely used methods in IPMSM drives include vector control methods, for example, direct torque control (DTC) [8], [9], field-oriented control (FOC) [10], [11], and adaptive control [12].

The maximum torque per ampere strategy (MTPA) strategy is often favoured [13], [14] to maximise the potential of the IPMSM, especially at speeds higher than the nominal speed; therefore, utilising flux weakening control is best to improve the speed, output torque, and dynamic responses [15].

With advantages such as simple algorithms, high reliability, and convenient parameter tuning, traditional proportional integral derivative (PID) or proportional integral (PI) controllers [16]-[18] are applied to many linear objectives; however, IPMSM is a nonlinear objective with external disturbances or variations in the internal parameters of the motor so the nonlinear controllers have been widely applied, for example, sliding mode control (SMC), backstepping (BSP), intelligent control, and adaptive control [13], [19]-[23].

Hashemi *et al.* [24] designed a PI controller based on neural networks combining flux weakening and MTPA to regulate the IPM's speed. Hamida *et al.* [25] used a BSP controller based on MTPA and a

high-gain adaptive observer to control IPM. Lin *et al.* [26], proposed a SMC to enhance the reliability against model uncertainties. Abdellah *et al.* [27] has applied linearisation technique for synchronous motors of electric vehicles. Laoufi *et al.* [28] designed a new model of SMC based on electric traction drive in-field control of IM powered by multi-level inverter.

However, the works as mentioned above have yet to propose or implement the integration of some methods in controlling IPM. Therefore, in this paper, the SMC with the exponential reaching control law along with the proportional-derivative term-ks will be designed for the speed loop of the IPMSM to enhance system stability while employing the MTPA algorithm and control in the flux weakening region to increase torque and expand the speed adjustment range. Finally, the validity and correctness of the proposed methods will be demonstrated through simulation results conducted by MATLAB/Simulink.

## 2. MODELING THE DRIVE SYSTEM OF THE ELECTRIC VEHICLE

### 2.1. Modeling interior permanent magnet synchronous motor

The stator voltage equation in the  $dq$  coordinate of the IPMSM can be expressed as (1) [13], [29]:

$$\begin{cases} U_{sd} = R_s I_{sd} + L_{sd} \frac{di_{sd}}{dt} - \omega_s L_{sq} i_{sq} \\ U_{sq} = R_s I_{sq} + L_{sq} \frac{di_{sq}}{dt} + \omega_s L_{sd} i_{sd} + \omega_s \psi_p \end{cases} \quad (1)$$

where  $U_{sd}$ ,  $U_{sq}$ ,  $i_{sd}$ ,  $i_{sq}$  are the stator voltages, currents on the  $dq$  coordinate;  $R_s$  is the stator resistance,  $L_{sd}$  and  $L_{sq}$  are the stator inductances,  $\omega_s$  is the angular velocity of the motor, and  $\psi_p$  is the permanent magnet flux. The electromagnetic torque can be calculated:

$$T_e = \frac{3}{2} p_p (\psi_p i_{sq} - i_{sd} i_{sq} (L_{sd} - L_{sq})) \quad (2)$$

with  $T_e$  is the motor's electric torque and  $p_p$  is the number of pole pairs.

The motion equation:

$$T_e - T_L = \frac{J}{p_p} \frac{d\omega_s}{dt} \quad (3)$$

where  $T_L$  and  $J$  are the load torque and the motor's inertia.

### 2.2. Modeling the forces acting on an electric vehicle

When a vehicle moves on the road, numerous factors influence its speed: air resistance, frictional force, gravity, and slope, as shown in Figure 1. Air resistance is calculated using (4):

$$F_w = \frac{1}{2} \rho C_d A (v_{veh} + v_w)^2 \quad (4)$$

where  $\rho$  is the air density;  $C_d$  is the coefficient of air resistance (typically:  $0.2 < C_d < 0.4$ );  $A$  is the frontal area of the vehicle's body (cross-sectional area);  $v_w$  is the wind velocity; and  $v_{veh}$  is the vehicle's velocity.

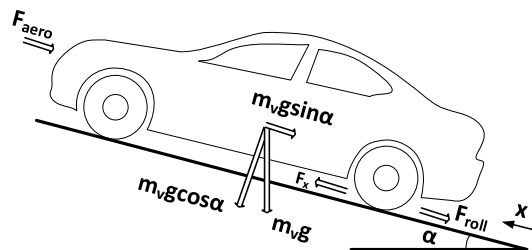


Figure 1. The forces acting on the car [30]

Rolling friction force can be calculated as (5):

$$F_r = f_r mg \cos \alpha \tag{5}$$

where  $m$  is the total mass of the vehicle and passengers;  $g$  is the gravitational acceleration;  $\alpha$  is the slope angle; and  $f_r$  is the coefficient of rolling resistance calculated by (6):

$$f_r = \frac{1}{100} + \frac{3.6}{10^4} v_{veh} \tag{6}$$

### 3. DESIGNING CONTROL FOR THE SPEED LOOP CIRCUIT COMBINING THE MAXIMUM TORQUE PER AMPERE STRATEGY METHOD IN THE FLUX WEAKENING REGION

The car operates at a speed higher than the rated speed, so the speed is controlled within the flux-weakening region while ensuring maximum torque. Therefore, the control structure, based on the principle of field-oriented control, consists of current loop circuits with PI controllers and SMC for the speed loop combined with the MTPA strategy, which is presented in Figure 2.

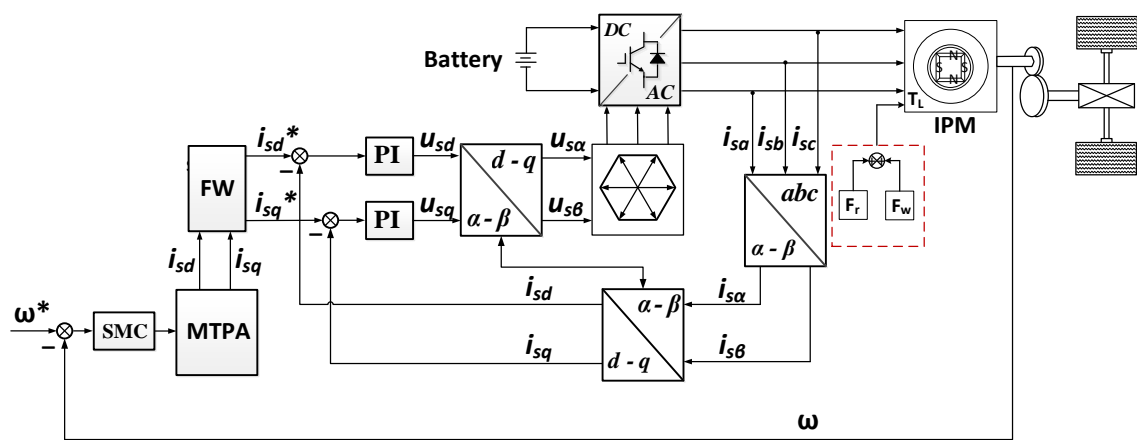


Figure 2. FOC control structure for IPMSM

#### 3.1. Maximum torque per ampere strategy

The essence of MTPA control lies in designing the current commands  $I_{sd}$  and  $I_{sq}$  with limited current and voltage conditions in Figure 3. When controlling  $i_{sd} < 0$ , the reluctance torque is utilized, increasing the motor's maximum torque. However, increasing the reluctance torque may affect the synchronous torque (which may decrease) due to the limitation of the stator current  $I_s$ . Therefore, we must solve the optimization problem to select the  $i_{sd}$  current command to achieve the maximum torque-to-current ratio  $(M/I_s)_{max}$ , throughout the operating speed range [31].

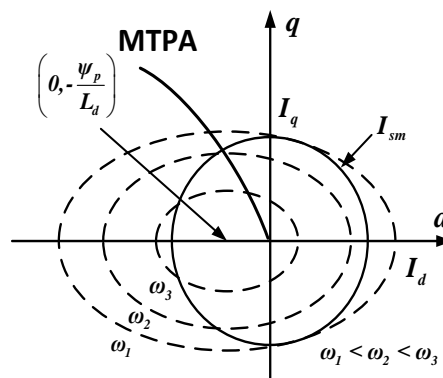


Figure 3. Limitations of voltage and current

Identifying constraints on current and voltage limits:

$$\begin{cases} I_s = \sqrt{i_{sd}^2 + i_{sq}^2} \leq I_{sm} \\ U_s = \sqrt{u_{sd}^2 + u_{sq}^2} \leq U_{sm} \end{cases} \quad (7)$$

We observe that the voltage limit values vary with speed, specifically:

$$U_s = \sqrt{(R_s i_{sd} - \omega_s L_{sq} i_{sq})^2 + (\omega_s \psi_p - R_s i_{sq} + \omega_s L_{sd} i_{sd})^2} \quad (8)$$

Approximately neglecting voltage drop across resistance, we have:

$$(L_{sq} i_{sq})^2 + (L_{sq} i_{sq} + \psi_p)^2 \leq \left(\frac{U_{sm}}{\omega_s}\right)^2 \quad (9)$$

In (9) shows the voltage limit characteristics depending on speed, and at a characteristic speed value, it forms an ellipse with coordinates at  $(0, -\psi_p/L_{sd})$  (dashed curve).

In (10) represents the MTPA curve [32]:

$$i_{sd} = \frac{\psi_p}{2(L_{sq}-L_{sd})} - \sqrt{\frac{\psi_p^2}{4(L_{sq}-L_{sd})^2} + i_{sq}^2} \quad (10)$$

In (10) represents the trajectory of the pairs of points  $(i_{sd}, i_{sq})$  that result in maximum torque. When operating at the above base speed, the current  $i_{sd}$  is described:

$$i_{sd} = \frac{-\psi_p}{L_{sd}} + \frac{1}{L_{sd}} \sqrt{\frac{U_{sm}^2}{\omega_s^2} - (L_{sq} i_{sq})^2} \quad (11)$$

We have the algorithm to calculate the reference values  $i_{sd}^*$  and  $i_{sq}^*$  according to MTPA as in Figure 4.

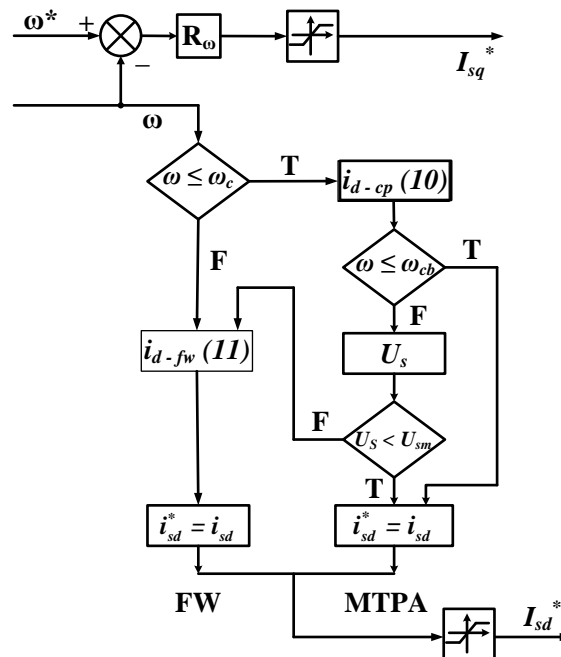


Figure 4. The algorithm to set the values of  $i_{sd}^*$  and  $i_{sq}^*$  for MTPA

### 3.2. Flux weakening method

The expression relating stator current and stator flux:

$$\psi_s = (\psi_p + L_{sd}i_{sd}) + jL_{sq}i_{sq} \quad (12)$$

Let's consider  $i_{sq}$  as the main current component generating torque and not varying much when the motor speed is steady. In this case, the flux linkage  $\psi_s$  can be reduced by pumping a current  $i_{sd}$  even more negative. Then, the reactive reaction along the excitation axis occurs more strongly, causing a decrease in the stator-side flux linkage.

Solving (9), we obtain the relationship:

$$i_{sd} = -\frac{\psi_p}{L_{sd}} + \frac{1}{L_{sd}} \sqrt{\left(\frac{U_{sm}}{\omega_s}\right)^2 - (L_{sq}i_{sq})^2} \quad (13)$$

When the speed reaches a nominal value, the voltage will reach the voltage  $U_{sm}$ . Therefore, to increase the speed further needs to reduce the flux  $\psi$ , which also means reducing torque. This is shown in Figure 5.

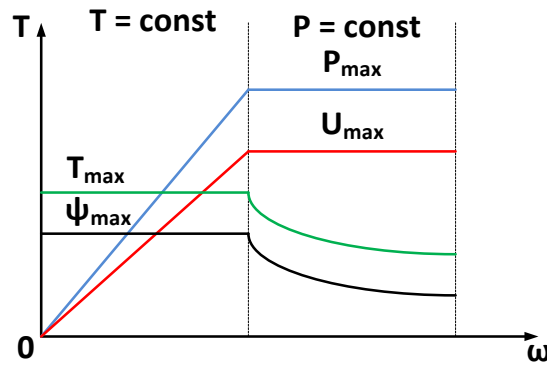


Figure 5. Characteristics of torque and power in nominal flux and weakening flux

### 3.3. The design of sliding mode control for speed loop

The SMC controller can be designed with various SMC laws to ensure the system's quality. According to [18], [33], some of the mentioned laws include:

The constant rate reaching law can be described in (14):

$$\dot{s}_1 = -\varepsilon \operatorname{sgn}(s), \varepsilon > 0 \quad (14)$$

$\varepsilon$  is the rate of approach to the switching point  $s=0$ . The advantage of this achieved law is its simplicity. However, if  $\varepsilon$  is tiny, the time to reach  $s$  will be prolonged; meanwhile, if  $\varepsilon$  is too large, the chattering phenomena will be severe.

The exponential reaching law can be written (15):

$$\dot{s}_1 = -\varepsilon \operatorname{sgn}(s) - ks, \varepsilon > 0, k > 0 \quad (15)$$

in which  $s=-ks$  is an exponential function and  $s=s(0)e^{-kt}$ . By adding the term proportional to  $-ks$ , the system state can approach sliding mode at a high rate when  $s$  is large.

The power rate reaching law can be described as (16):

$$\dot{s}_1 = -k|s|^\alpha \operatorname{sgn}(s), k > 0, 0 < \alpha < 1 \quad (16)$$

small control gains can be ensured to decrease chattering by choosing  $\alpha$  when the system state is far from the sliding mode, i.e. When  $s$  is large.

The general reaching law can be described in (17):

$$\dot{s}_1 = -\varepsilon \operatorname{sgn}(s) - f(s), \varepsilon > 0 \quad (17)$$

where  $f(0)=0$  and  $sf(s)>0$  when  $s\neq 0$ .

The design of SMC: the speed error  $e$  is expressed as (18):

$$e = \omega - \omega^* \quad (18)$$

where  $\omega^*$  is the reference speed and  $\omega$  is the feedback speed.

The first-order derivative of the error yields:

$$\dot{e} = \dot{\omega} - \dot{\omega}^* = \frac{p_p}{J}(T_e - T_L) - \dot{\omega}^* \quad (19)$$

The sliding surface  $s$  is defined:

$$s = ce + \dot{e} \quad (20)$$

Taking the derivative of the sliding surface, we obtain:

$$\dot{s} = c\dot{e} + \ddot{e} = c\left(\frac{p_p}{J}(T_e - T_L) - \dot{\omega}^*\right) + \ddot{e} \quad (21)$$

Selecting the Lyapunov function:

$$V = \frac{1}{2}s^2 \quad (22)$$

The exponential reaching law is selected in (23):

$$\dot{s} = -\varepsilon \operatorname{sgn}(s) - ks, \varepsilon > 0, k > 0 \quad (23)$$

From (20) and (22), we have:

$$\begin{aligned} c\left(\frac{p_p}{J}(T_e - T_L) - \dot{\omega}^*\right) + \ddot{e} = -\varepsilon \operatorname{sgn}(s) - ks &\Leftrightarrow \frac{p_p}{J}(T_e - T_L) = -\frac{\varepsilon}{c}\operatorname{sgn}(s) - \frac{k}{c}s + \dot{\omega}^* \Leftrightarrow T_e = \\ \frac{-\frac{\varepsilon}{c}\operatorname{sgn}(s) - \frac{k}{c}s + \dot{\omega}^* + \frac{p_p}{J}T_L}{\frac{p_p}{J}} = \frac{J}{p_p}\left(-\frac{\varepsilon}{c}\operatorname{sgn}(s) - \frac{k}{c}s + \dot{\omega}^*\right) + T_L \end{aligned} \quad (24)$$

The derivative of  $V$  yields.

$$\begin{aligned} \dot{V} &= s \cdot \dot{s} = s(c\dot{e} + \ddot{e}) = s\left[c\left(\frac{p_p}{J}(T_e - T_L) - \dot{\omega}^*\right) + \ddot{e}\right] \\ &= s\left\{c\left[\frac{p_p}{J}\left(\frac{J}{p_p}\left(-\frac{\varepsilon}{c}\operatorname{sgn}(s) - \frac{k}{c}s + \dot{\omega}^*\right) + T_L\right) - \frac{p_p}{J}T_L\right]\right\} \\ &= s(-ks - \varepsilon \operatorname{sgn}(s)) = -(\varepsilon|s| + ks^2) \leq 0 \end{aligned} \quad (25)$$

#### 4. SIMULATION AND EVALUATION OF RESULTS

The simulation parameters are presented in two tables. Table 1 presents IPMSM's parameters in a certain electric car, while Table 2 presents the parameters of the electric vehicle and the environment's parameters. The speed reference curve is chosen from the Economic Commission for Europe (ECE) reference curve.

Table 1. The parameters of the IPMSM

Parameters	Value
Stator resistance, $R_s$	6.5e-3 Ohm
d-axis inductance, $L_{sd}$	1.597e-3 H
q-axis inductance, $L_{sq}$	2.057e-3 H
Moment of inertia, $J$	0.09 kg.m <sup>2</sup>
Number of pole pairs, $p_p$	4
DC voltage, $V_{dc}$	550 V

Table 2. The parameters of the auto

Parameters	Value
Vehicle weight+load	2018 kg
Wheel radius	0.3 m
Transmission ratio	9.73
Maximum speed	130 km/h
Effective area	2.3 m <sup>2</sup>
Air density	1.25 kg/m <sup>3</sup>
Road gradient	0
Rolling resistance coefficient	0.02

Figure 6 illustrates the speed response curve when using the SMC controller. The feedback speed closely tracks the set speed. We abruptly change the load to test the system's stability at time  $t=65$  s. With a sudden change of load, the speed undergoes slight oscillations for a short period of time  $t=0.2$  s but then quickly converges to the set curve. This indicates that the system can remain stable with the SMC control method despite disturbances and external parameters.

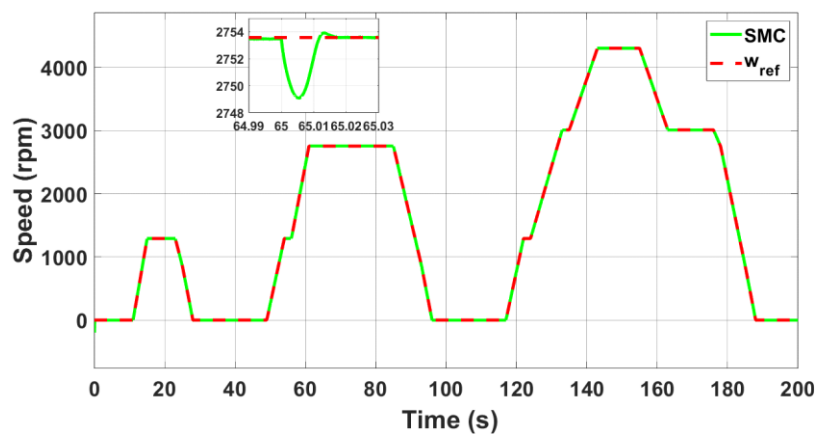


Figure 6. The speed response of the electric vehicle drive control system

For electric vehicles, the flux needs to be adjusted to increase speed beyond the rated speed. When the motor operates above the rated speed (here at 1,200 rpm), as shown in Figure 7, we can observe a decrease in torque when the speed exceeds 1,200 rpm. This helps electric vehicles operate stably at high speeds with high efficiency.

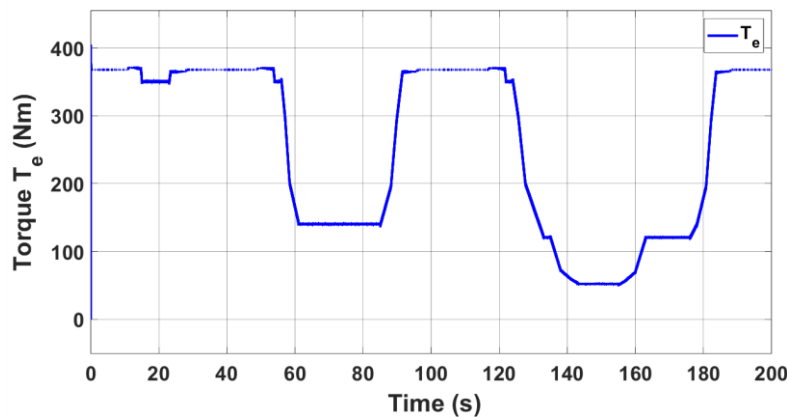


Figure 7. The torque response

The output of the MTPA and flux weakening blocks is the set current values  $i_{sd}$  and  $i_{sq}$ . Figure 8 shows a pretty good response to the current. The two currents,  $i_{sd}$  and  $i_{sq}$ , have been separated, and the current  $i_{sd}$  has been controlled to be less than 0. Additionally, since  $i_{sq}$  controls the torque, the formulas for calculating  $i_{sd}$  and  $i_{sq}$  in the flux weakening block have been computed for  $i_{sd} < 0$  and  $i_{sq}$  decreasing.

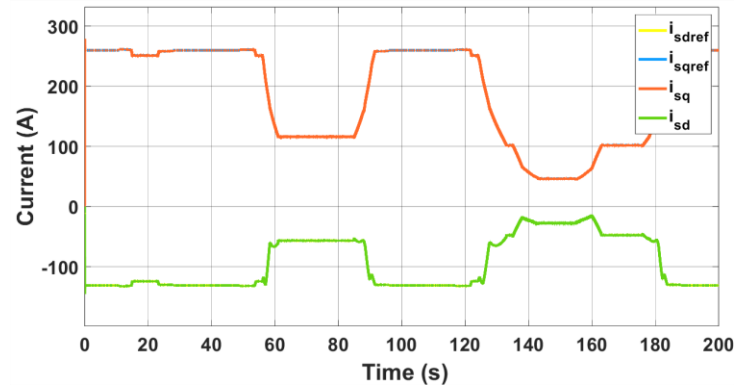


Figure 8. Responses of the currents  $i_{sd}^*$ ,  $i_{sq}^*$  and  $i_{sd}$ ,  $i_{sq}$

## 5. CONCLUSION

The paper proposed a SMC method combined with the MTPA control strategy on the current ratio in the flux-weakening region to control the speed of the IPM motor in electric vehicles. Simulation results using MATLAB/Simulink software have demonstrated that the SMC has provided a fairly good speed response. Additionally, with MTPA, the motor torque has been improving, enabling the motor to operate efficiently at high speeds. This proves that the proposed control method for controlling the IPM motor operating at speeds above the rated speed is feasible and effective. The results of this paper have also highlighted the critical role of integrating modern control methods such as SMC, MTPA algorithm. By leveraging the advantages of each method, we have developed a robust and flexible control system for IPM motors in electric vehicles, thereby improving the system's performance and responsiveness.

## ACKNOWLEDGEMENTS

We would like to thank Thuyloi University and the University of Transport and Communications for their financial support for our research.




## REFERENCES

- [1] C. C. Chan, A. Bouscayrol, and K. Chen, "Electric, hybrid, and fuel-cell vehicles: architectures and modeling," *IEEE Transactions on Vehicular Technology*, vol. 59, no. 2, pp. 589-598, 2010, doi: 10.1109/TVT.2009.2033605.
- [2] V. T. Buyukdegirmenci, A. M. Bazzi, and P. T. Krein, "Evaluation of induction and permanent magnet synchronous machines using drive-cycle energy and loss minimization in traction applications," *IEEE Transactions on Industry Applications*, vol. 50, no. 1, pp. 395-403, 2014, doi: 10.1109/TIA.2013.2266352.
- [3] D. G. Dorrell, A. M. Knight, M. Popescu, L. Evans and D. A. Staton, "Comparison of different motor design drives for hybrid electric vehicles," *2010 IEEE Energy Conversion Congress and Exposition*, Atlanta, GA, USA, 2010, pp. 3352-3359, doi: 10.1109/ECCE.2010.5618318.
- [4] X. Liu, Z. Q. Zhu and D. Wu, "Evaluation of efficiency optimized variable flux reluctance machine for EVs/HEVs by comparing with interior PM machine," *2014 17th International Conference on Electrical Machines and Systems (ICEMS)*, Hangzhou, China, 2014, pp. 2648-2654, doi: 10.1109/ICEMS.2014.7013948.
- [5] P. G. Pellegrino, A. Vagati, B. Boazzo, and P. Guglielmi, "Comparison of induction and PM synchronous motor drives for EV application including design examples," *IEEE Transactions on Industry Applications*, vol. 48, no. 6, pp. 2322-2332, Nov.-Dec. 2012, doi: 10.1109/TIA.2012.2227092.
- [6] J. Goss, M. Popescu, and D. Staton, "A comparison of an interior permanent magnet and copper rotor induction motor in a hybrid electric vehicle application," *2013 International Electric Machines & Drives Conference*, Chicago, IL, USA, 2013, pp. 220-225, doi: 10.1109/IEMDC.2013.6556256.
- [7] J. H. Seo and H. S. Choi, "Cogging torque calculation for IPM having single layer based on magnetic circuit model," *IEEE Transactions on Magnetics*, vol. 50, no. 10, pp. 1-4, Oct. 2014, Art no. 8102104, doi: 10.1109/TMAG.2014.2327204.
- [8] Y. Zhang and J. Zhu, "Direct torque control of permanent magnet synchronous motor with reduced torque ripple and commutation frequency," *IEEE Transactions on Power Electronics*, vol. 26, no. 1, pp. 235-248, Jan. 2011, doi: 10.1109/TPEL.2010.2059047.
- [9] M. M. Ndoumbé et al, "DTC with fuzzy logic for multi-machine systems: traction applications," *International Journal of Power*






- Electronics and Drive Systems (IJPEDS)*, vol. 12, no. 4, pp. 2044-2058, 2021, doi: 10.11591/ijped.v12.i4.pp2044-2058.
- [10] A. H. Memon and I. A. Rahman, "High-speed current dq PI controller for vector controlled PMSM drive," *The Scientific World Journal*, vol. 2014, pp. 1-9, 2014, doi: 10.1155/2014/165158.
- [11] C. S. T. Dong, H. H. Le, and H. H. Vo, "Field oriented controlled permanent magnet synchronous motor drive for an electric vehicle," *International Journal of Power Electronics and Drive Systems (IJPEDS)*, vol. 14, no. 3, pp. 1374-1381, 2023, doi: 10.11591/ijped.v14.i3.pp1374-1381.
- [12] H. H. Choi, V. Q. Leu, Y.-S. Choi, and J.-W. Jung, "Adaptive speed controller design for a permanent magnet synchronous motor," *IET Electric Power Applications*, vol. 5, no. 5, pp. 457-464, 2010, doi: 10.1049/iet-epa.2010.0083.
- [13] P. Hou, X. Wang, and Y. Sheng, "Research on flux-weakening control system of interior permanent magnet synchronous motor based on fuzzy sliding mode control," in *2019 Chinese Control And Decision Conference (CCDC)*, Nanchang, China, 2019, pp. 3151-3156, doi: 10.1109/CCDC.2019.8832483.
- [14] A. Dianov, K. Young-Kwan, L. Sang-Joon, and L. Sang-Taek, "Robust self-tuning MTPA algorithm for IPMSM drives," in *2008 34th Annual Conference of IEEE Industrial Electronics*, Orlando, FL, USA, 2008, pp. 1355-1360, doi: 10.1109/IECON.2008.4758151.
- [15] Z. Xinghua, T. Qitai, and W. Ting, "Direct torque control of interior permanent magnet synchronous motor with maximum torque per ampere," in *2016 IEEE 11th Conference on Industrial Electronics and Applications (ICIEA)*, Hefei, China, 2016, pp. 1519-1524, doi: 10.1109/ICIEA.2016.7603826.
- [16] F. Hui, Z. Yuefei, L. Chuang, and Z. Jie, "A variable structure PI controller for permanent magnetic synchronous motor speed-regulation system," *Transactions of China Electrotechnical Society*, vol. 30, no. 12, pp. 237-242, 2015.
- [17] B. Li, and Y. Z. Feng, "Researching of speed regulation system for AC permanent magnet synchronous motor," *Applied Mechanics and Materials*, vol. 303-306, pp. 1204-1208, 2013, doi: 10.4028/www.scientific.net/AMM.303-306.1204.
- [18] L. Feng, M. Deng, S. Xu and D. Huang, "Speed regulation for PMSM drives based on a novel sliding mode controller," *IEEE Access*, vol. 8, pp. 63577-63584, 2020, doi: 10.1109/ACCESS.2020.2983898.
- [19] A. A. A. Samat and M. N. Fazli, "Regular paper speed control design of permanent magnet synchronous motor using Takagi-Sugeno fuzzy logic control," *Journal of Electrical Systems*, vol. 13, no. 4, p. 689-695, 2017.
- [20] A. J. S. Ali and G. P. Ramesh, "Neural network-controlled wind generator-fed  $\Gamma$ -Z source-based PMSM drive," *Artificial Intelligence and Evolutionary Computations in Engineering Systems*, vol. 517, pp. 387-396, 2017, doi: 10.1007/978-981-10-3174-8\_34.
- [21] Z. Song, X. Mei, T. Tao, and M. Xu, "The sliding-mode control based on a novel reaching technique for permanent magnet synchronous motors," *Electric Power Components and Systems*, vol. 47, no. 16-17, pp. 1505-1513, 2019, doi: 10.1080/15325008.2019.1663299.
- [22] M. Aqib, R. Mehmood, A. Alzahrani, I. Katib, A. Albeshri, and S. M. Altowaijri, "Smarter traffic prediction using big data, in-memory computing, deep learning and gpus," *Sensors*, vol. 19, no. 9, 2019, doi: 10.3390/s19092206.
- [23] T. D. Chuyen *et al.*, "Improving control quality of PMSM drive systems based on adaptive fuzzy sliding control method," *International Journal of Power Electronics and Drive Systems (IJPEDS)*, vol. 13, no. 2, pp. 835-845, 2022, doi: 10.11591/ijped.v13.i2.pp835-845.
- [24] Z. Hashemi, M. Mardaneh, and M. S. Sadeghi, "High performance controller for interior permanent magnet synchronous motor drive using artificial intelligence methods," *Scientia Iranica*, vol. 19, no. 6, pp. 1788-1793, 2012, doi: 10.1016/j.scient.2012.07.001.
- [25] M. A. Hamida, J. De Leon, and A. Glumineau, "Experimental sensorless control for IPMSM by using integral backstepping strategy and adaptive high gain observer," *Control Engineering Practice*, vol. 59, pp. 64-76, 2017, doi: 10.1016/j.conengprac.2016.11.012.
- [26] C.-K. Lin, T.-H. Liu, M.-Y. Wei, L.-C. Fu, and C.-F. Hsiao, "Design and implementation of a chattering-free non-linear sliding-mode controller for interior permanent magnet synchronous drive systems," *IET Electric Power Applications*, vol. 6, no. 6, pp. 332-344, 2011, doi: 10.1049/iet-epa.2011.0040.
- [27] B. Abdellah, H. Abdeldjebar, and K. Medjdoub, "An application for nonlinear control by input-output linearization technique for pm synchronous motor drive for electric vehicles," *International Journal of Power Electronics and Drive Systems*, vol. 13, no. 4, pp. 1984-1992, 2022, doi: 10.11591/ijped.v13.i4.pp1984-1992.
- [28] C. Laoufi, Z. Sadoune, A. Abbou, and M. Akherraz, "New model of electric traction drive based sliding mode controller in field-oriented control of induction motor fed by multilevel inverter," *International Journal of Power Electronics and Drive Systems*, vol. 11, no. 1, pp. 242-250, 2020, doi: 10.11591/ijped.v11.i1.pp242-250.
- [29] Z. Zhang and X. Liu, "A duty ratio control strategy to reduce both torque and flux ripples of DTC for permanent magnet synchronous machines," *IEEE Access*, vol. 7, pp. 11820-11828, 2019, doi: 10.1109/ACCESS.2019.2892121.
- [30] B. K. Bose, *Modern power electronics and AC drives*, Prentice Hall, 2002.
- [31] N. P. Quang and J.-A. Dittrich, "Vector control of three-phase AC machines," *System Development in the Practice*, 2<sup>nd</sup>. Edition, Springer Berlin Heidelberg, 2015, doi: 10.1007/978-3-662-46915-6.
- [32] K. Ueda, S. Morimoto, Y. Inoue, and M. Sanada, "A novel control method in flux-weakening region for efficient operation of interior permanent magnet synchronous motor," *IEEJ Journal of Industry Applications*, vol. 4, no. 5, pp. 619-625, 2015, doi: 10.1541/ieejia.4.619.
- [33] J. Liu and X. Wang, *Advanced sliding mode control for Mechanical Systems*, Springer Berlin Heidelberg, 2011, doi: 10.1007/978-3-642-20907-9.




**BIOGRAPHIES OF AUTHORS**

**An Thi Hoai Thu Anh**    received her engineer (1997) and M.Sc. (2002) degrees in industrial automation engineering from Hanoi University of Science and Technology and completed Ph.D. degree in 2020 from The University of Transport and Communications (UTC). Now, she is a lecturer at the Faculty of Electrical and Electronic Engineering at the University of Transport and Communications (UTC). Her current interests include power electronic converters, electric motor drive, and saving energy solutions applied for industry and transportation. She can be contacted at email: [htanh.ktd@utc.edu.vn](mailto:htanh.ktd@utc.edu.vn).



**Tran Hung Cuong**    received his engineer (2010); and M.Sc. (2013) degrees in industrial automation engineering from Hanoi University of Science and Technology and completed Ph.D. degree in 2020 from Hanoi University of Science (HUST). Now, he is a lecturer at the Faculty of Electrical and Electronic Engineering at Thuy Loi University (TLU). His current interests include power electronic converters, electric motor drives, converting electricity from renewable energy sources to the grid, saving energy solutions applied for the grid and transportation. He can be contacted at email: [cuongth@tlu.edu.vn](mailto:cuongth@tlu.edu.vn).



**Duong Minh Chien**    is a fourth-year student majoring in electrical engineering at the University of Transport and Communications (UTC), Vietnam. His current interests include power electronics control and electric drive control applied in the transportation and the industry. He can be contacted at email: [chien201503731@lms.utc.edu.vn](mailto:chien201503731@lms.utc.edu.vn).